Learning Based Interpretable End-to-End Control Using Camera Images

Sandesh Athni Hiremath, Praveen Kumar Gummadi, Argtim Tika, Petrit Rama and Naim Bajcinca
Department of Mechanical and Process Engineering, Rheinland-Pfälzische Technische Universität Kaiserslautern-Landau, Gottileb-Daimler-Straße 42, 67663 Kaiserslautern, Germany

Keywords: Autonomous Driving, MPC, Learning Based Control, End-to-End Control, Lane Detection.

Abstract: This work proposes a learning-based controller for an autonomous vehicle to follow lanes on highways and motorways. The controller is designed as an interpretable deep neural network (DNN) that takes as input only a single image from the front-facing camera of an autonomous vehicle. To this end, we first implement an image-based model predictive controller (MPC) using a DNN, which takes as input 2D coordinates of the reference path made available as image pixels coordinates. Consequently, the DNN based controller can be seamlessly integrated with the perception and planner network to finally yield an end-to-end interpretable learning-based controller. Here, all of the controller components, namely- perception, planner, state estimation, and control synthesizer, are differentiable and thus capable of active and event-triggered adaptive training of the relevant components. The implemented network is tested in the CARLA simulation framework and then deployed in a real vehicle to finally demonstrate and validate its performance.

1 INTRODUCTION

An autonomous driving system consists of various sub-systems, starting from environment perception, localization, scene understanding, decision-making, and controller (Thrun et al., 2006). Every sub-system outputs intermediate results and representations, which are very important for tracing decisions, interpretation, and improving the overall performance of the system. However, this approach is often time-consuming and also lacks global consistency, as modules are optimised for intermediate results rather than the end task. To remedy this, inspired by the works of (Pomerleau, 1988) (T. Jochem and D. Pomerleau, 1995) (LeCun et al., 2005) and driven by recent advancements in data-driven and deep learning methods (Bojarski et al., 2016) (Codevilla et al., 2019) (Bansal et al., 2019) (Natan and Miura, 2023), researchers are focusing on developing robust end-to-end approaches, where all modules are optimized for the end task. One major issue that arises in end-to-end approaches is the lack of explainability and interpretability of intermediate outputs. The recent learning-based approaches that dominate the methodology for implementing end-to-end algorithms suffer from this problem.

Modular approaches, such as conventional solutions, have the advantage of interpretability for each involved sub-modules, thus useful for fault detection in case of unexpected system behavior. Although the sub-modules are developed separately, they are tightly coupled and interdependent. Hence, it demands domain expertise and additional time to integrate and maintain the whole pipeline. In autonomous driving, this is especially the case for perception, data fusion, and localization modules. An overview covering these modules, their technical and functional aspects, as well as the main challenges, is presented in (Velasco-Hernández et al., 2020). On the other hand, an overview of approaches and challenges about planning and decision-making modules for self-driving vehicles, is presented in (Schwarting et al., 2018).

Although control modules can be realized independently or jointly as a single integrated framework with the path planning, they are nonetheless tightly coupled with the perception and state estimation layers. This makes it challenging to obtain a generalized and robust system behavior. As an optimization-based control technique, model predictive control (MPC) is widely used in automated systems to plan an optimal trajectory or follow a given reference path. MPC exhibits high structural flexibility in defining quality and target criteria by means of a cost function and state/input constraints. These jointly ensure that system-relevant limits are adhered to, thus ensuring safe operation. Focusing on path tracking for automated road vehicles, (Stano et al., 2022) provides a comprehensive overview and classification of dif-

Hiremath, S., Gummadi, P., Tika, A., Rama, P. and Bajcinca, N.
Learning Based Interpretable End-to-End Control Using Camera Images.
DOI: 10.5220/0012206500003543
In *Proceedings of the 20th International Conference on Informatics in Control, Automation and Robotics (ICINCO 2023) - Volume 1*, pages 474-484
ISBN: 978-989-758-670-5; ISSN: 2184-2809

ferent MPC formulations published in recent years. Particularly in autonomous driving, many researchers make use of MPC for path planning or path following control (Paden et al., 2016) (Weiskircher et al., 2017) (Ji et al., 2017) (Alcala et al., 2020). The proposed algorithms are validated mainly by simulations, considering different driving scenarios. In (Kim et al., 2021), an MPC-based approach with a variable prediction horizon is proposed, where experiments with a real vehicle at low speed are performed in addition to simulations in CARLA. A learning-based MPC using Gaussian process regression to improve the vehicle model online is presented in (Kabzan et al., 2019) and tested on the AMZ race car (Kabzan et al., 2020).

Compared to modular methods, end-to-end approaches solve the problem of autonomous driving as a single module, from feature extraction/engineering to decision-making and control algorithms. This approach maps input data from the vehicle's sensors to the output of low-level control commands, such as steering, braking, and acceleration. The overall architecture is unified and acts as a black box without submodules and intermediate outputs. However, due to a lack of meaningful intermediate outputs, the system's explainability is lower, and therefore harder to trace its decision or the root cause of an error. Moreover, this approach raises challenges such as the requirement of bigger models, thus larger computation overhead, for obtaining sufficiently robust encoded features and for fusing information across different sensor modalities.

One of the earliest neural networks, ALVINN, dating back to 1989, was trained end-to-end for predicting steering angle from camera and radar images for the task of lane following on public roads without human intervention (Pomerleau, 1988). In 1995, a project named "No Hands Across America" was proposed, training an end-to-end model for lane keeping, mapping video images to steering angle, assisted by a human driver to control the acceleration and braking of the vehicle (T. Jochem and D. Pomerleau, 1995). DAVE, a small robot car, was proposed to avoid obstacles and navigate using image inputs. It also was trained as an end-to-end convolutional neural network (CNN) to predict steering angles for off-road vehicle control (LeCun et al., 2005). End-to-end approaches came again in prominence when NVIDIA proposed a large-scale CNN for learning meaningful road features in order to solve the entire task of lane following by steering the vehicle in different environments and weather conditions (Bojarski et al., 2016). Another end-to-end algorithm is introduced in (Hecker et al., 2018) to learn low-level car maneuvers from realistic inputs of surround-view cameras. More recently, in (Xiao et al., 2023), the authors have used CNN and long short-term memory (LSTM) along with a differentiable control barrier network for vision-based end-to-end autonomous driving. However, it relies on the availability of a nominal controller that generates feasible controls.

Another simple form of end-to-end learning is imitation learning (IL), an approach for training autonomous driving systems by imitating an expert human driver, i.e., steering, acceleration, or braking (Codevilla et al., 2019). Although it works well for simple scenarios of lane following, this approach faces difficulties in complex traffic scenarios since using just the image as an input is not enough to predict high-level maneuvers or to map the input into low-level vehicle control commands. To address these problems, conditional IL is introduced in (Codevilla et al., 2018) by mapping the input of the planned maneuver, apart from the perception input, into the control signal of steering angle and acceleration at training time. Planned maneuvers are also used as an input in (Xiao et al., 2022), experimenting with multimodality of perception data and different stages of data fusion for conditional IL. A further IL framework is presented in (Bansal et al., 2019) by synthesizing trajectory perturbation and augmenting undesirable behavior to increase the robustness of the model. It is also worth mentioning the interesting work of (Chen et al., 2022), where a Bayesian interpreted reinforcement learning (RL) method is proposed for end-to-end learning in urban scenarios. This, however, involves latent variables which are difficult to physically interpret thus troublesome for debugging.

Taking advantage of both approaches, we propose a novel end-to-end approach in which perception, planning, state estimation, and control modules are implemented in a differentiable manner via the use of DNNs. As a result, we retain the interpretability of intermediate outputs and gain robustness of DNNs and tuning flexibility to meet global system performance. This end-to-end learnable and interpretable framework takes images as input, and produces controls and future trajectories of the ego-vehicle as outputs. The perception module detects static features of the road in the form of lane markings and delivers them as the primary information for navigation. The intermediate output from the perception module and planner serves as a candidate reference target for the controller, thus interpretable. The feedback (state estimation) layer not only filters out a suitable trajectory for the ego-vehicle but also estimates the vehicle's current state. Altogether, the involved modules, namely- lane detection, planning, state estimation, and controller, are jointly optimizable for the end

task of lane following. The developed model is validated by testing on a real vehicle.

The remainder of the paper is organized as follows. The addressed problem is defined in Sec. 2. The proposed end-to-end control approach, including all its components, is described in Sec. 3. Sec. 4 presents the implementation architecture and experimentation results. In Sec 5, we discuss the results and provide some concluding remarks.

2 PROBLEM DEFINITION

In this work, we consider the problem of lane following by an autonomous vehicle equipped with a single front-facing camera. To this end, we first provide an MPC formulation, which on one hand, serves as a mathematical representation of the lane following task, and on the other hand, serves as a foundation for developing an end-to-end learning-based controller.

Let $X \in \mathbb{R}^{d_x}$, $U \in \mathbb{R}^{d_u}$, $Y \in \mathbb{R}^{d_y}$ denote the state, control and output variables, respectively, of a dynamical system and expressed with respect to (w.r.t) O_v, the vehicle coordinate system. Let $F : \mathbb{R}^{d_x} \times \mathbb{R}^{d_u} \to \mathbb{R}^{d_x}$ and $H : \mathbb{R}^{d_x} \times \mathbb{R}^{d_u} \to \mathbb{R}^{d_y}$ be C^1 functions, i.e. continuously differentiable functions. Based on this let the dynamics of the system be specified by

$$\begin{aligned} \dot{X}(t) &= F(X(t),U(t)), t > 0, \\ Y(t) &= H(X(t),U(t)), t \geq 0, \\ X(0) &= \mathrm{x}. \end{aligned} \tag{1}$$

Let $\mathcal{X}$, $\mathcal{Y}$, and $\mathcal{U}$ denote the sets of admissible states, outputs, and controls, respectively. Let $\mathrm{Y}(t) \in \mathcal{Y}$ denote the target path of the vehicle and $G(t) \in \mathcal{G}$ denote the environmental constraints on the vehicle, then the path following problem can be posed as the task of finding an optimal control $U(t) \in \mathcal{U}$ such that the vehicle with the current state x reaches the target path $\mathrm{Y}(t) \in \mathcal{Y}$ while adhering to the environmental constraint $G(t) \in \mathcal{G}$ in the fixed time horizon $[t, t+T_h]$, $t, T_h > 0$. Mathematically, this can be formulated as the following optimal control problem (OCP):

$$\begin{aligned} J(X,U;\mathrm{Y}) &= \int_0^{T_h} e^{s\lambda} \|H(X,U) - \mathrm{Y}(s)\|^2_{Q_Y} \, ds \\ &\quad + \int_0^{T_h} e^{s\lambda} \|U(t+s)\|_{Q_U} \, ds, \\ X^*(t), U^*(t) &= \underset{X \in X, U \in \mathcal{U}}{\operatorname{argmin}} \; J(X,U;\mathrm{Y}), \\ \frac{dX}{ds}(t+s) &= F(X(t+s),U(t+s)), s \in (0,T_h] \\ X(t) &= \mathrm{x}(t), \; X(t+s) \leq G(t+s). \end{aligned} \tag{2}$$

Solving (2) for each time step t using the data $\mathrm{Y}(t), G(t)$ and $\mathrm{x}(t)$ obtained from planning, perception and feedback modules, respectively, we obtain the standard MPC algorithm. Thus, the general sequence of steps required to solve the lane following task are (i) perceive, (ii) plan, and (iii) control. Since, as mentioned above, we are interested in devising an end-to-end learning based algorithm and also offering good interpretability of outputs, we design each of the above mentioned modules as neural networks. The designed networks are such that when combined, they form a single computational chain. Consequently, it facilitates back-propagation of the prediction errors up to the input layer, thereby enabling end-to-end, i.e., output-to-input learning mechanism. To this end, we have implemented four neural networks, which are then combined together to obtain a single *end-to-end interpretable image-based controller* network, which we refer to as the *EyeCon* network (shortly as *EyeConNet*). The first two components of *EyeConNet* are the camera based lane-detection and virtual trajectory generation (VTG) networks, named together as LDVTG. The next (third) component is the feedback network (shortly as FB) which provides the mechanism for estimating the state of the vehicle based on the features obtained from the input camera image, mainly from the output of the LDVTG. Finally, the fourth component is the controller network, called the VehCon, which serves as the model predictive controller. Altogether, combining the four, as depicted in Fig. 3, yields an interpretable network for the task of following the lane by using only a single front-facing camera. To the best of our knowledge, the proposed approach for designing a tuneable autonomous controller that uses only a camera image as the input and whose behavior is validated on a real vehicle and real roads has not been made before.

3 COMPONENTS OF THE EyeCon NETWORK

3.1 Perception and Planning Network

The core perception task for lane following is lane detection. To this end, we rely on the existing work of Ultra Fast Structure-aware Deep Lane Detection (UFLD) (Qin et al., 2020). Although it works quite well on regular RGB images, it showed poor performance on images obtained from our vehicle. The UFLD model trained on TuSimple dataset (TuS, 2023) (even with CuLane and CurveLanes dataset) did not provide stable and continuous lane detection across the frames obtained from our test vehicle. We

argue that the reason for this is the difference in camera settings (i.e., high saturation, brightness, etc.) between the camera from our test vehicle and the camera used to obtain the images of the TuSimple dataset. To overcome this problem, we collected and labeled approximately 1200 images with the front-facing camera of our test vehicle and used them to fine-tune the model. After this step, as evident in Fig. 1, the detections were consistent and stable across video frames obtained while driving.

Since UFLD outputs detection probabilities across downscaled columns for four lanes and for fixed row anchor positions, in order to obtain lane and trajectory coordinates, we introduce two custom layers that constitute the VTG network (or layer). The algorithmic steps of VTG network (or layer) are as follows: (i) for each row and lane-type filter out low probability detections, (ii) do a softmax across columns and scale it (based on image resolution) to obtain column position, (iii) sort the tensor based on a reverse ordering of row index, so that the bottom-most pixel (denoting near field) is first, while the top most pixel (denoting far field) is last, and finally (iv) resample the tensor to have fixed number of pixels for each of the four lanes. Based on the fixed number of lane coordinates for each lane, we perform the weighted sum of adjacent lane coordinates to obtain the lane-following trajectory. Consequently, the output of VTG is four lanes and three trajectory coordinates. The above-mentioned operations are implemented in a differentiable manner and without disrupting the computation graph.

(a) Detected lanes by UFLD.

(b) Ego lanes and trajectory.

Figure 1: Outputs from UFLD (left image) and the VTG (right image). The left image shows the detected lanes of UFLD after training on TuSimple (orange) and fine-tuning on RPTU (dark purple) datasets, respectively. The right image shows the ego lane (dark purple) and the generated ego trajectory (green).

3.2 Controller

In this section, we introduce a novel learning based control algorithm for the problem of lane following. We rely on the above MPC formulation based on the OCP (2) to achieve this. Accordingly, given $\mathbf{x} := (\mathrm{x}, \mathrm{Y}, G)$, where x is the current state of the vehicle, Y is the reference trajectory and G is the environmental constraints, the solution U^* to the OCP (2) can be written as a mapping $\mathbf{x} \mapsto \mathfrak{M}(\mathbf{x})$ with $U^* := \mathfrak{M}(\mathbf{x})$. From this perspective, a practically convenient way to implement a learning based controller is to train a DNN to learn the mapping $\mathbf{x} \mapsto \mathfrak{M}(\mathbf{x})$. We do so via the following steps: (i) we set up a kinematic model, which serves as a prediction (state propagation) model, and (ii) we implement a network for the generation of optimal controls.

3.2.1 Vehicle Kinematic Model (VKM)

The motion of the vehicle on a 2D road is modeled at the kinematic level so that the network is easily generalizable and thus be applicable to any nonholonomic front axle steered vehicles. Since we are interested in trajectory tracking, we follow the approach of (Weiskircher et al., 2017) to model the kinematics in the Frenet coordinate system given by the prescribed trajectory. Following this, the error dynamics of the vehicle is expressed in the Frenet frame O_s of the reference path. Letting ψ_s and ψ_p denote the orientation of the reference frame and course angle of the vehicle, the yaw-error ψ_e is defined as $\psi_e = \psi_p - \psi_s$. The distance of the vehicle to the reference path along n_s denotes the lateral distance and thus represents the lateral error of the vehicle w.r.t the reference path. Its dynamics is given as: $\dot{y}_e = v_t \sin(\psi_e)$ where v_t is the instantaneous velocity experienced at the vehicle's center of gravity (CoG). Similarly, the yaw-error dynamics $\dot{\psi}_e$ can be given as: $\dot{\psi}_e = \dot{\psi}_p - \dot{s}\kappa$ with $\dot{s} = v_t \cos(\psi_e)(\frac{1}{1-y_e\kappa})$. Here, s denotes the length along the reference trajectory and $\kappa = 1/\rho$ denotes the curvature of the reference path, with ρ being the radius of the circle of instantaneous rotation (CIR). Introducing the control variables a_t and α, which denote longitudinal acceleration and yaw rate of the CoG respectively, the dynamics of the planar motion of the

vehicle is given by the equations:

$$\begin{aligned} \dot{y}_e &= v_t \sin(\psi_e),\ \dot{\psi}_e = \alpha_p - \frac{v_t \cos(\psi_e)\kappa}{(1-y_e\kappa)}, \\ \dot{v}_t &= a_t,\ \dot{\psi}_p = \alpha,\ \dot{s} = \frac{v_t \cos(\psi_e)}{(1-y_e\kappa)}, \\ \dot{x} &= v_t \cos(\psi_p),\ \dot{y} = v_t \sin(\psi_p). \end{aligned} \tag{3}$$

Let $U = [a_t, \alpha]^\top \in \mathbb{R}^2$ denote the control vector and

$$X = [X_1, \ldots, X_7]^\top = [v_t, \psi_p, s, \psi_e, y_e, x, y]^\top \in \mathbb{R}^7$$

denote the state vector of the vehicle, the VKM can be compactly written in the form of (3) where H is a suitable matrix such that

$$H(X,U) = H(X) = [v_t, \psi_e, y_e, x, y]^\top \in \mathbb{R}^5.$$

Based on this and denoting $\mathfrak{s} := \{e, c, p, dc, dp\}$, the cost function J for the associated MPC formulation reads as

$$\begin{aligned} J(X,U;\mathrm{Y}) &= \gamma_e L_e(X) + \gamma_p L_p(X,\mathrm{Y}) + \gamma_c L_c(U) \\ &\quad + \gamma_{dp} L_{dp}(X) + \gamma_{dc} L_{dc}(U), \end{aligned} \tag{4}$$

$$L_e(X) = \sum_{n=1}^{N_{T_h}-1} e^{n\lambda} \|X_e(t_n)\|^2_{Q_e} + \lambda_e \|X_e(t_{N_{T_h}})\|^2_{Q_e},$$

$$L_c(U) = \sum_{n=1}^{N_{T_h}-1} e^{n\lambda} \|U_{t_n}\|^2_{Q_c} + \lambda_c \|U(t_{N_{T_h}})\|^2_{Q_c},$$

$$\begin{aligned} L_p(X,\mathrm{Y}) &= \sum_{n=2}^{N_{T_h}-1} e^{n\lambda} \|X_p(t_n) - \mathrm{Y}(t_n)\|^2_{Q_p} \\ &\quad + \lambda_p \|X_p(t_{N_{T_h}}) - \mathrm{Y}(t_{N_{T_h}})\|^2_{Q_p}, \end{aligned}$$

$$L_{dp}(X) = \sum_{n=2}^{N_{T_h}} e^{n\lambda} \|X(t_n) - X(t_{n-1})\|^2_{Q_{dp}},$$

$$L_{dc}(U) = \sum_{n=2}^{N_{T_h}} e^{n\lambda} \|U(t_n) - U(t_{n-1})\|^2_{Q_{dc}}.$$

where, $N_{T_h} \in \mathbb{N}$ is the number of discrete points for the time horizon $[t, t+T_h]$, $t_n = t + \frac{nT_h}{N_{T_h}}$, $X_e = [\psi_e, y_e]^\top$ denotes the error vector, $X_p = [v_t, x, y]^\top$ denotes the tangential speed and position vector. The quantities λ_j, Q_j for $j \in \mathfrak{s}$, denotes the scaling factor and weighting matrices for the loss terms.

3.2.2 Network Architecture

The controller network (VehCon) is designed as a stacked recurrent network composed of Gated-Recurrent-Units (GRUs). An i-th GRU cell, $\mathfrak{N}_{Z_i}$, takes as input the i-th component of the input-data Y_i and G_i to generate the estimate $\hat{Z}_i$, which is then fed to $\mathfrak{N}_U$, a fully connected network whose weights are shared across temporal points, to obtain the control $\hat{U}_i$ for i-th time step. The output of the network is the sequence of controls $\hat{U}$ and the states $\hat{X}$ predicted by the controls. Since the control network is designed to play the role of a statistical optimizer, its loss functional $\mathfrak{L}$ is based on J (4) and is given as

$$\begin{aligned} \mathfrak{L}(X,U,\mathrm{Y}) &:= \mathbb{L}(X,U,\mathrm{Y}) + \gamma_{rb}\mathbb{L}_{rb}(X,U,\mathrm{Y}), \\ \mathbb{L}(X,U,\mathrm{Y}) &:= J(X,U;\mathrm{Y}), \end{aligned} \tag{5}$$

$$\mathbb{L}_B(X,G) := \frac{\gamma_G}{\varepsilon_B + \|X-G\|^2},\ \varepsilon_B := .001,$$

$$\mathbb{L}_{rb}(X,U,\mathrm{Y}) := \rho([L_p, L_e, L_c, L_{de}, L_{dc}, \mathbb{L}_B]^\top),$$

$$Q_p = \mathrm{diag}([q_v, q_x, q_y]^\top), \quad Q_e = \mathrm{diag}([q_{\psi_e}, q_{y_e}]^\top),$$

$$Q_c = \mathrm{diag}([q_{a_t}, q_\alpha]^\top), \quad \Lambda = [\lambda, \lambda_p, \lambda_e, \lambda_c]^\top$$

where, $\mathbb{L}_B$ is acting as a barrier function that handles environmental constraints, ρ is a parameterized robust-loss-functional (Barron, 2019). Altogether, the VehCon is composed of 174 K learning parameters that amounts to 837 KB of memory consumption. Next, the data required for training the statistical optimization solver is synthetically generated by appropriately sampling the inputs from the valid range. Based on this $\mathrm{x} \in \mathcal{U}([-1,1])$, Y a local trajectory for the vehicle, is obtained by parameterizing with respect to the curvature κ, which is uniformly sampled from $[-.1, .1]$. The generated trajectories are set to have lane-boundaries at fixed lateral distances. In this manner, we generate a generic dataset to cover all possible (local) maneuvers of the vehicle. Furthermore, we also collect the reference trajectories and feedback input predicted by the LDVTG and FB networks on the RPTU test dataset. The former serves for robust stand-alone training of the control network, while the latter serves for fine-tuning it on the outputs of the preceding components of the EyeConNet. Both datasets are as shown in Fig. 2.

3.3 Feedback Network

The feedback network or layer (FB) is an important component of EyeConNet that is responsible for estimating the current state of the vehicle using only the information obtained from the image features. The feedback layer takes as input the lane and trajectory coordinates (i.e. the output of VTG) and provides as output (i) the ego reference and lane coordinates and (ii) an estimate of the current vehicle state $\hat{X}(t)$. The former is obtained by selecting the lane and trajectory (triplet) having more than a required number of coordinates, which then serve as the ego or reference

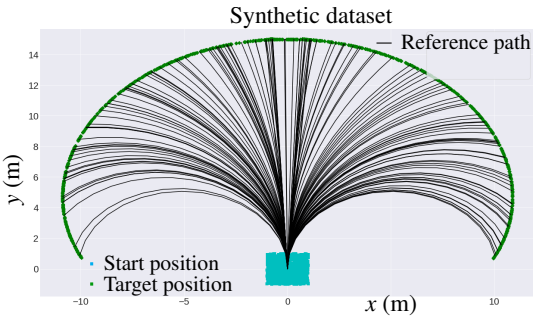

(a) Training samples.

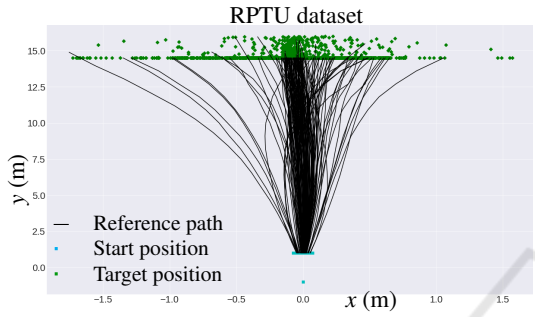

(b) RPTU data samples.

Figure 2: Samples from dataset consisting of reference trajectories (black), start positions (cyan) and target end (green) positions.

(triplet) coordinates. In this way, FB is also acting as a naive decision-making layer. Once the ego triplet, consisting of a pair of lane coordinates and reference trajectory coordinates, are obtained, the ego trajectory is used to estimate the state vector $\hat{X}(t)$. Firstly, since we want to generate the trajectory local to the vehicle, we transform the pixels from the image coordinate system to the vehicle coordinate system O_v. Consequently, this has the added benefit that some of the components of the state vector remain fixed, i.e. $\hat{\psi}_p = \pi/2$, $\hat{y} = 0$ and $\hat{x} = -x_{vs}$ with $x_{vs} := 2$m denoting the fixed look ahead distance of the camera. The error components $X_e := [y_e(t), \psi_e(t)]^\top$ is estimated as follows. Let $\mathrm{y}_i = (u_i, v_i)^\top$ denote the i-th coordinate of the ego trajectory in vehicle coordinate, then $\hat{y}_e \approx -\frac{k_{y_e}}{n}\sum_i^n u_i$ and $\hat{\psi}_e \approx -\arctan([k_{\psi_e}, u_n - u_0]^\top)$ with $k_{y_e} > 0$ and $k_{\psi_e} \geq 1$ acting as tuning parameters. Based on testing and simulation we set $k_{y_e} = 5$ and $k_{\psi_e} = 2$. Next, the curvature $\kappa_p(t)$ of the virtual trajectory is obtained by using the parameterized curvature formula, where derivatives are approximated by finite differences. Based on this, the current estimate $\hat{X}(t)$ of the vehicle state X at time t, w.r.t O_v, is given as $[v_t^o, \frac{\pi}{2}, 0, \psi_e, y_e, 0, -x_{vs}]^\top$. Here, v_t^o is the open-loop estimate of the vehicle velocity obtained by integrating (starting from the previous state) the acceleration signal or from the IMU sensor. Similar to VTG, the operations of FB are implemented in a differentiable manner and do not consists of any learnable parameters.

3.4 Training Methodology

To train the EyeConNet, we follow a three stage approach. In the first stage (Stage1) we train the LDVTG, i.e., the UFLD and VTG networks, to obtain stable lane detections and virtual trajectories. In the second stage (Stage2) we use the predictions of the LDVTG on the RPTU test-set as the training set and finetune the VehCon. This is analogous to detaching the computation graph of the VehCon from the rest of EyeConNet while training. The parameters involved in (4) and (5) for training the VehCon are as described in Table 1. The Stage2 training mainly facilitates in adapting the VehCon, which was pretrained on a generic vehicle kinematics dataset (see Fig. 2), for the distribution of feedback inputs generated by the VTG. Subsequently, in the third stage (Stage3) we combine VehCon and LDVTG to obtain the EyeConNet, and train it on the combined dataset of TuSimple and RPTU. For the unified training of EyeConNet, the learnable parameters of the networks are the ones belonging to ULFD and VehCon, since, in the current implementation, the VTG and FB do not have any learnable parameters. Based on this, the loss function for the joint training is given by $\mathfrak{L}_{EyeCon} = \mathfrak{L}_{UFLD} + 0.3\mathfrak{L}_{VehCon}$, where $\mathfrak{L}_{VehCon}$ is given by (5) and $\mathfrak{L}_{UFLD}$ is as in (Qin et al., 2020). The evaluation scores, on the joint test set of RPTU and TuSimple, for each training stage are tabulated in Table 2. For comparison, we have also mentioned the baseline score obtained by using pretrained (TuSimple) weights of the UFLD network. Firstly, the result of Stage1 training (second row of Table 2) indicates that both fine-tuning (warm start) and fresh training (cold start) of LDVTG network on the joint dataset do not quantitatively alter the results much. However, as depicted in Fig. 1, there is a significant increase in the quality in terms of pixel-wise and frame-wise continuity of the detected lanes on RPTU images. Next, the result of Stage2 training (third row of Table 2) is indicated by the RMSE value of the error vector $[\psi_e, y_e]$ evaluated at the terminal time, $t + T_h$, of the prediction horizon. The obtained value of 0.123 is small enough (i.e. $y_e < 15$cm and $\psi_e < .1$ degree) to proceed with the next stage of training. Subsequently, in Stage3 for training the EyeConNet we used the pretrained weights of the VehCon from Stage2. Here, we performed experiments by warm starting and cold starting the LDVTG, wherein the former uses the baseline weights or starts fresh. Additionally, we also

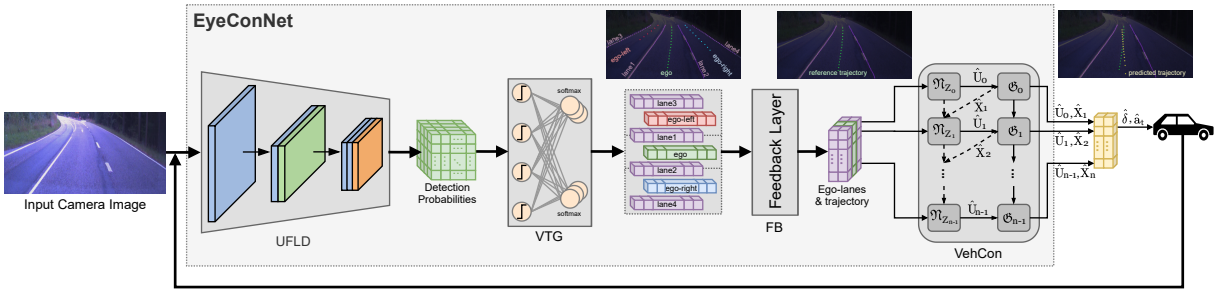

Figure 3: Network architecture of EyeConNet, an end-to-end lane following controller network.

Table 1: Parameter values relating to the loss function $\mathfrak{L}$ (5).

$\lambda = 0.02$	$\lambda_p = 20$	$\lambda_e = 20$	$\lambda_c = .5$	$q_v = 10^3$
$q_y = .05$	$q_{\psi_e} = 10$	$q_{y_e} = 2$	$q_{a_t} = .01$	$q_\alpha = 5$
$\gamma_{rb} = 1$	$\gamma_c = 1$	$\gamma_{dp} = 1$	$\gamma_{dc} = 10^{-3}$	$\gamma_e = 10^{-5}$
$\gamma_G = .005$	$\gamma_p = 10^{-5}$	$q_x = 2$		

experimented by having the computation graph for the controller network either detached or joined with the rest of the network. The former is referred to as Stage3.0, and the latter as Stage3.1. Based on the evaluation scores of each training stage tabulated in Table 2, we see that firstly, cold start training is better than the warm start, i.e., using pretrained UFLD weights (baseline) is not quantitatively advantageous. Secondly, we notice that detached training of VehCon ensures that LDVTG has almost the same performance as that of the Stage1. This is to say that the risk of deterioration of LDVTG due to multi-tasked training of EyeConNet is reduced to almost zero by having the VehCon in detached mode while training. Consequently, the result of VehCon for Stage3 is similar to that of Stage2 with Stage3.0 showing slightly better and the Stage3.1 slightly worse performance. Looking at Fig. 5 and Fig. 6, we see that the generated controls are well-behaved in the sense that the error states $[\psi_e, y_e]^\top$ are smoothly reduced to zero along the prediction horizon such that the error distribution at the end of the prediction horizon has the mean value close to zero. Furthermore, from Fig. 7, we can also infer that generated acceleration and yaw rates are smooth and decay to zero along the prediction horizon. These qualitative properties, along with good prediction results from EyeConNet, as depicted in Fig. 4, assure confidence for deploying it on the vehicle and testing it on real scenarios.

Table 2: Stage wise training results for network components.

Training Stages	Fine Tuning (warm start)		Fresh Training (cold start)		RMSE
	Acc	**F1-S**	**Acc**	**F1-S**	
Baseline	95.82%	87.88%	-	-	
Stage1	95.60%	87.54%	95.27%	87.23%	-
Stage2	-	-	-	-	0.123
Stage3.0	95.6%	87.4%	**95.8%**	**87.8%**	**0.118**
Stage3.1	85.4%	62.5%	86.5%	66.4%	0.124

4 IMPLEMENTATION AND RESULTS

The proposed algorithms are tested and validated on an VW Passat, which has been modified to perform autonomous driving experiments, see Fig. 8. The experimental vehicle is equipped with power management, computational, environment sensing, and communication resources, including CAN-bus-based reading and writing access to the vehicle data, respectively, vehicle actuators. In this work, perception is based on a single camera directed toward the roadway. The control algorithms are implemented in PYTHON on a CarPC with NVIDIA A2 GPU and Intel Core i7-8700T Processor with a clock rate of 2.40GHz. Since EyeConNet is implemented using the PyTorch framework, it was easily deployed in CarPC. Furhtermore, to compare its performance, we also implemented the standard MPC problem using the CasADi framework (Andersson et al., 2019) and the resulting optimization problem, i.e., the OCP (2), is solved with the IPOPT solver (Wächter and Biegler, 2006).

A schematic of the lane following controller implemented in the vehicle is shown in Fig. 9. The perception module takes input from the camera and pro-

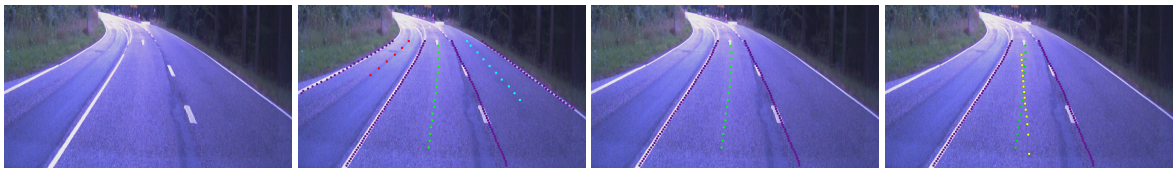

(a) Input Image. (b) Virtual trajectories. (c) Selected ego trajectory. (d) Predicted vehicle path.

Figure 4: Prediction result of EyeConNet on a sample test image.

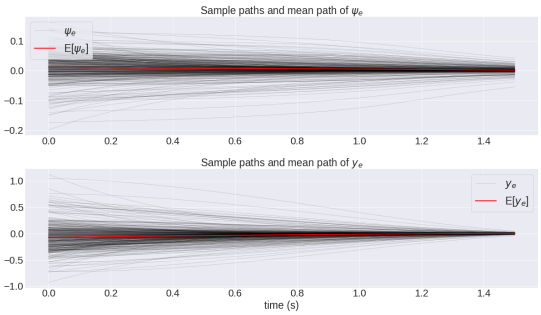

Figure 5: Predicated error states ψ_e and y_e.

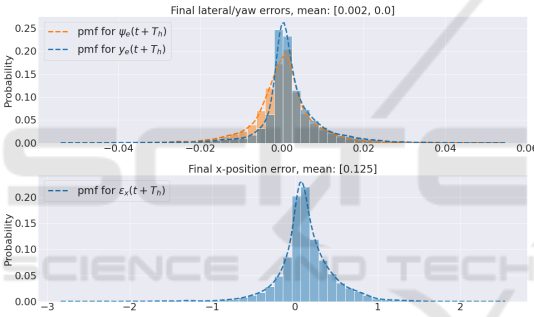

Figure 6: Error distributions of terminal position and orientation of the vehicle.

vides the reference trajectory for the controller, which then, following the idea presented in Section 3.2, synthesizes optimal values for the vehicle longitudinal acceleration $\hat{a}_t$ and the yaw rate $\hat{\psi}_p$. The perception block is nothing but the LDVTG, while the controller block is the VehCon or a classical MPC-based controller. Note that here we have, on purpose, decou-

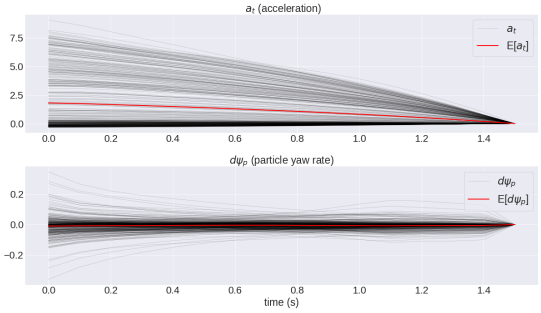

Figure 7: Generated controls

Figure 8: Experimental vehicle.

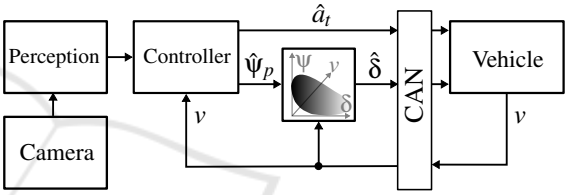

Figure 9: Schematics of the vehicle control architecture.

pled the perception and controller block to facilitate the integration of the classical MPC with the LDVTG. The controller takes the current velocity of the vehicle as a feedback and uses it to update the state estimate from FB. Furthermore, the obtained yaw rate $\hat{\psi}_p$ is converted to the corresponding steering angle $\hat{\delta}$ using a three-dimensional function approximation previously generated from measurements at different vehicle speeds.

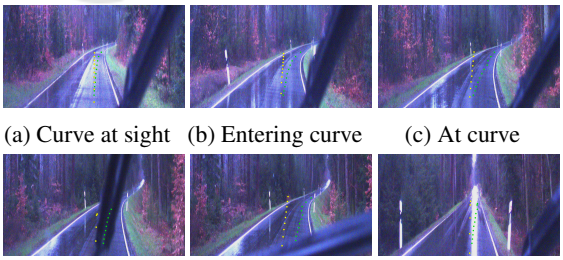

(a) Curve at sight (b) Entering curve (c) At curve

(d) Visual block (e) Exiting curve (f) Successful exit

Figure 10: Curve maneuver of EyeCon at 54 kmph under poor visibility and heavy rain.

4.1 Results

In this section, we mainly focus on the experimental results performed with our experimental vehicle VW Passat (see Fig. 8). Albeit, before proceeding

to vehicle testing, we indeed tested EyeConNet in CARLA for two different map environments namely Town04 and Town06. In this test, the EyeConNet was able to detect the lanes for more than 95% of the frames and the detections were also sequentially stable. Consequently, the generated local trajectory was always within the lane boundary and even centered. As a result, the VehConNet was successful in following the generated reference path successfully and reliably, which subsequently encouraged us to go ahead with the real vehicle testing. For the real-world testing, we performed tests on a public country-side road that had sufficient good lane markings. The tests are performed for two target velocity speeds, 36km/h and 54km/h. For safety reasons, we have avoided testing at higher speeds. In order to validate the perception and planner module, i.e., the LDVTG, we also perform the same tests using a standard MPC controller. This also serves as a comparison candidate for the VehCon. The obtained results are as depicted in Fig. 11. Based on this, we can observe the following: (i) at the global vehicle behavior level, both MPC and EyeConNet based controllers were able to achieve the task of lane following. The drive-experience was stable and pleasant, without any abrupt behavior. The stable behavior of MPC indicates that LDVTG and FB were sufficiently good in providing reliable lane detections, reference trajectory, and state estimates. (ii) The performance of the VehCon (DNN controller) is in close comparison with that of the MPC. The traversed trajectory in both cases was nearly identical (as seen in the top left corner, blue vs. orange path) for both target velocities. The high-level profile of the steering angle is also similar for both controllers. This is to say that the turning maneuvers match each other and also the road profile. At higher speeds, the magnitude of steering is relatively higher in comparison to the lower speed. Furthermore, the VehCon is more reactive to turns in the sense that it aligns to a turn earlier and is thus marginally better at sharper turns. Looking at the velocity profiles, we see that both controllers are able to reach the respective target velocities pretty quickly and are able to maintain it. However, the VehCon seems to be slightly aggressive and tends to overshoot the reference. This is explainable from the control profiles generated by VehCon on the test set, which indicates a clear bias for positive values, depicted in the upper plot of Fig. 7. Despite this, we did not observe a deteriorating effect on the controller performance. Altogether, the interpretable architecture of EyeConNet provides satisfactory performance and offers robust validation and testing mechanism. Furthermore, it also enabled the computation time for each of the network components to be measured during the closed loop operation of the controller. This is tabulated in Table 3. As per that, we see that perception and planning together take under 15 ms in total, with perception being around 5 ms and planning around 9 ms, respectively, on average. The state estimation is even faster, with under 2 ms of runtime, while the control synthesizer takes the most time, around 32.5 ms on average. Consequently, all the modules combined, the total runtime is under 50 ms, which we believe to be quite good for the complexity of the task being considered.

Table 3: Mean computation times of network components.

UFLD	VTG	FB	VehCon	Total
5 ms	9 ms	1.5 ms	32.5 ms	48 ms

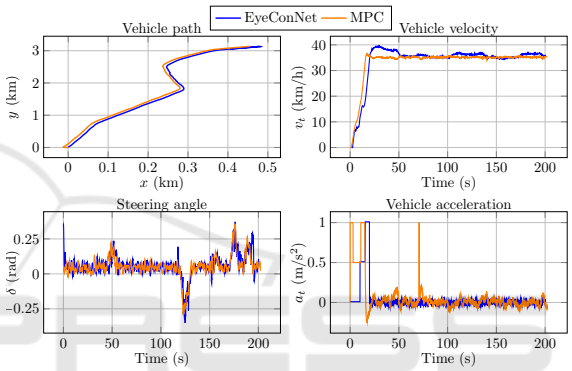

(a) Results of experiment with 36 kmph as target velocity.

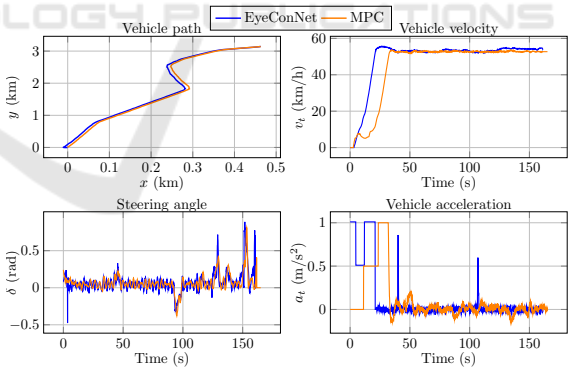

(b) Results of experiment with 54 kmph as target velocity.

Figure 11: Comparison of Vehicle performance at different target speeds of 36kmph (10m/s) and 54kmph (15m/s) when fed with VehCon and MPC derived controls respectively.

5 CONCLUSION

In this paper, we have proposed an end-to-end interpretable image based DNN controller called EyeConNet, capable of steering and accelerating the vehicle

directly from the image information. The modular and interpretable design of EyeConNet not only allowed us to train it incrementally, keeping the performance of the fused network equal to that of their standalone counterparts, but also allowed seamless integration with the classic MPC controller, enabling robust and comparative testing. The developed network was initially tested in CARLA, then subsequently tested on real public roads while adhering to safety requirements. The obtained performance for EyeConNet was satisfactory and in good comparison with a classical MPC controller. The stable performance of MPC, when fed with LDVTG outputs, reassures the stable performance of the perception and planner modules, thanks to stage-wise training and finetuning on images obtained from vehicle-specific cameras. Furthermore, testing during rainy weather and low visibility conditions, both MPC and EyeConNet were able to show respectable performance (see Fig. 10) with minor deterioration, i.e., occasional deactivation of the control interface due to lack of reference trajectory due to failure of LDVTG. Lastly, a highly competitive runtime of under 50 ms of EyeConNet, on the one hand, encourages us to consider even more complex models to increase robustness and, on the other hand, to consider active-closed-loop learning with either MPC or driver in the loop. The latter opens up a lot of interesting research problems, especially in the area of IL and RL.

ACKNOWLEDGEMENTS

This work was supported by the German Federal Ministry of Transport and Digital Infrastructure (BMDV) within the scope of the project AORTA with the grant number 01MM20002A.

REFERENCES

Tusimple: Tusimple benchmark. https://github.com/TuSimple/tusimple-benchmark. Accessed: 2023-03-15.

Alcala, E., Sename, O., Puig, V., and Quevedo, J. (2020). Ts-mpc for autonomous vehicle using a learning approach. *IFAC-PapersOnLine*, 53(2):15110–15115. 21st IFAC World Congress.

Andersson, J. A. E., Gillis, J., Horn, G., Rawlings, J. B., and Diehl, M. (2019). CasADi – A software framework for nonlinear optimization and optimal control. *Mathematical Programming Computation*, 11(1):1–36.

Bansal, M., Krizhevsky, A., and Ogale, A. S. (2019). Chauffeurnet: Learning to drive by imitating the best and synthesizing the worst. In *Robotics: Science and Systems XV, University of Freiburg, Freiburg im Breisgau, Germany, June 22-26, 2019*.

Barron, J. T. (2019). A general and adaptive robust loss function. *CVPR*.

Bojarski, M., Testa, D. D., and et al. (2016). End to end learning for self-driving cars. *CoRR*, abs/1604.07316.

Chen, J., Li, S. E., and Tomizuka, M. (2022). Interpretable end-to-end urban autonomous driving with latent deep reinforcement learning. *IEEE Transactions on Intelligent Transportation Systems*, 23(6):5068–5078.

Codevilla, F., Müller, M., López, A. M., Koltun, V., and Dosovitskiy, A. (2018). End-to-end driving via conditional imitation learning. In *International Conference on Robotics and Automation, ICRA*, pages 1–9. IEEE.

Codevilla, F., Santana, E., López, A. M., and Gaidon, A. (2019). Exploring the limitations of behavior cloning for autonomous driving. In *International Conference on Computer Vision, ICCV 2019*, pages 9328–9337. IEEE.

Hecker, S., Dai, D., and Gool, L. V. (2018). End-to-end learning of driving models with surround-view cameras and route planners. In *European Conference on Computer Vision, ECCV*, volume 11211 of *Lecture Notes in Computer Science*, pages 449–468. Springer.

Ji, J., Khajepour, A., Melek, W. W., and Huang, Y. (2017). Path planning and tracking for vehicle collision avoidance based on model predictive control with multiconstraints. *IEEE Transactions on Vehicular Technology*, 66(2):952–964.

Kabzan, J., Hewing, L., Liniger, A., and Zeilinger, M. N. (2019). Learning-based model predictive control for autonomous racing. *IEEE Robotics and Automation Letters*, 4(4):3363–3370.

Kabzan, J., Valls, M. I., and et al. (2020). Amz driverless: The full autonomous racing system. *Journal of Field Robotics*, 37(7):1267–1294.

Kim, M., Lee, D., Ahn, J., Kim, M., and Park, J. (2021). Model predictive control method for autonomous vehicles using time-varying and non-uniformly spaced horizon. *IEEE Access*, 9:86475–86487.

LeCun, Y., Muller, U., and et al. (2005). Off-road obstacle avoidance through end-to-end learning. In *Advances in Neural Information Processing Systems 18, NIPS*, pages 739–746.

Natan, O. and Miura, J. (2023). End-to-end autonomous driving with semantic depth cloud mapping and multi-agent. *IEEE Trans. Intell. Veh.*, 8(1):557–571.

Paden, B., Čáp, M., and et al. (2016). A survey of motion planning and control techniques for self-driving urban vehicles. *IEEE Transactions on Intelligent Vehicles*, 1.

Pomerleau, D. (1988). ALVINN: an autonomous land vehicle in a neural network. In Touretzky, D. S., editor, *Advances in Neural Information Processing Systems 1, [NIPS Conference, Denver, Colorado, USA, 1988]*, pages 305–313. Morgan Kaufmann.

Qin, Z., Wang, H., and Li, X. (2020). Ultra fast structure-aware deep lane detection. In *European Conference on Computer Vision*, pages 276–291. Springer.

Schwarting, W., Alonso-Mora, J., and Rus, D. (2018). Planning and decision-making for autonomous vehicles.

Stano, P., Montanaro, U., and et al. (2022). Model predictive path tracking control for automated road vehicles: A review. *Annual Reviews in Control*.

T. Jochem and D. Pomerleau (1995). No hands across america official press release. Carnegie Mellon University.

Thrun, S., Montemerlo, M., and et al. (2006). Stanley: The robot that won the DARPA grand challenge. *J. Field Robotics*, 23(9):661–692.

Velasco-Hernández, G. A., Yeong, D. J., Barry, J., and Walsh, J. (2020). Autonomous driving architectures, perception and data fusion: A review. In Nedevschi, S., Potolea, R., and Slavescu, R. R., editors, *16th IEEE International Conference on Intelligent Computer Communication and Processing, ICCP 2020, Cluj-Napoca, Romania, September 3-5, 2020*, pages 315–321. IEEE.

Weiskircher, T., Wang, Q., and Ayalew, B. (2017). Predictive Guidance and Control Framework for (Semi-)Autonomous Vehicles in Public Traffic. *IEEE Transactions on Control Systems Technology*, 25(6):2034–2046.

Wächter, A. and Biegler, L. (2006). On the implementation of an interior-point filter line-search algorithm for large-scale nonlinear programming. *Mathematical programming*, 106:25–57.

Xiao, W., Wang, T.-H., and et al. (2023). Barriernet: Differentiable control barrier functions for learning of safe robot control. *IEEE Transactions on Robotics*, 39(3):2289–2307.

Xiao, Y., Codevilla, F., Gurram, A., Urfalioglu, O., and López, A. M. (2022). Multimodal end-to-end autonomous driving. *IEEE Trans. Intell. Transp. Syst.*, 23(1):537–547.